Subgrain Formation during Deformation: Physical Origin and Consequences

R. SEDLÁČEK, W. BLUM, J. KRATOCHVÍL, and S. FOREST

The formation of subgrains in the course of plastic deformation is explained as a result of a trend to make the deformation easier by locally reducing the number of active slip systems. Local preference of one slip system changes the crystal orientation with respect to stress (Schmid factor), thus leading to geometrical softening or hardening. The trend to subgrain formation is treated in the framework of continuum mechanics as an instability against internal bending for the simple case of a crystal originally oriented for symmetric double slip. Once formed, the boundaries of the subgrains lead to hardening as they induce long-range internal back stresses in the interior of the subgrains by forcing the mobile dislocations to take a bowed configuration. Simple dislocation-based and Cosserat models are recalled to explain the size-dependent subgrain hardening, where smaller subgrains are stronger.

I. INTRODUCTION

MANY models of plasticity work with average dislocation densities that are the same everywhere in the crystal. While it is certainly a legitimate first step to build a model on this simplifying assumption, such models exclude the formation of deformation-induced dislocation structures and misorientations within a crystal that are important features of plastic deformation. The formation of misorientations leads to a structure of crystallites within the deforming grains that are bounded by dislocation networks in the form of subgrain boundaries or, as deformation proceeds to large strains and the misorientations increase, even by large angle boundaries. In fact, the buildup of misorientations during deformation has even led to the method of producing so-called nanocrystalline materials by severe plastic deformation. In the following, we will use the term subgrain structure to address the misoriented structure. This term is established in the field of creep where stresses are relatively low due to high temperature and the subgrain boundaries come close to ideal small angle boundaries. However, we do not mean that the subgrain boundaries resulting from the dislocation evolution during plastic deformation are ideal. Due to the fact that the crystal approaches a state of dynamic equilibrium, there is always some disturbance of the ideal state. Prolonged annealing after deformation brings the subgrain boundaries into a much more ideal state. The disturbance of the ideal structure increases with decreasing temperature. In cold working, the disturbance is so large that one does not usually use the term subgrain boundary but speaks of cell boundaries, distinguishing between various kinds, such as geometrically necessary and incidental boundaries. However, all kinds of boundaries are similar in that they constitute dislocation networks, which evolve during deformation from "thick" walls with high dipole content to "thin" essentially two-dimensional (2-D) walls, and in that they are associated with misorientations. From this point of view, there is no real need for a difference in nomenclature, except if one wants to differentiate between boundaries of different kinds and physical origin.

The present article addresses two questions. One is the question for the physical origin of the misorientations. The second is for the effect of the boundaries on deformation, once they have formed.

II. PHYSICAL ORIGIN OF SUBGRAIN FORMATION

A. *Primary-Secondary Hardening*

1. *Qualitative arguments*

In a homogeneously deforming body each volume element would perform the same change of shape. Therefore, there would be no misfit between the volume elements, and consequently, no need for misorientation between neighboring elements. This means that deformation must be inhomogeneous for misorientations to develop.

Plastic deformation by dislocation motion is heterogeneous by nature. The very existence of a dislocation line represents this heterogeneity. The fact that dislocations need sources for their generation within a crystal is another argument for heterogeneity. It is well known from observations of slip lines at the crystal surfaces that dislocations move in groups over a slip zone. However, the heterogeneity that leads to subgrain formation does not simply reflect slip zones. Slip zones are 2-D. They might well be distributed in a homogeneous manner over the crystal. Such distribution would not lead to misorientations between neighboring crystal volumes. Subgrains result from the fact that the slip activity on a given slip system is not the same in volume elements measuring about $20bG/\sigma$ (b: Burgers vector length; G: shear modulus; and σ: applied stress). This would imply that slip zones should be stacked one upon the other to create such a volume.

R. SEDLÁČEK, Research Assistant, is with the Lehrstuhl für Mechanik, TU-München, 85747 Garching, Germany. W. BLUM, Professor, is with the Institut für Werkstoffwissenschaften, Universität Erlanger-Nürnberg, 91058 Erlangen, Germany. J. KRATOCHVÍL, Professor, is with the Faculty of Civil Engineering, Department of Physics, Czech Technical University Prague, 166 29 Prague, Czech Republic. S. FOREST, Research Assistant is with the Centre des Matériaux, CNRS, Ecole des Mines de Paris, 91003 Evry, France.

This article is based on a presentation made in the workshop entitled "Mechanisms of Elevated Temperature Plasticity and Fracture," which was held June 27–29, 2001, in San Diego, CA, concurrent with the 2001 Joint Applied Mechanics and Materials Summer Conference. The workshop was sponsored by Basic Energy Sciences of the United States Department of Energy.

It should be noted that the deviation from homogeneity of deformation on each slip system is not very large. If slip was confined to a single slip system in each subgrain the misorientation, Θ, would equal the shear, γ, for small strains. This would mean $\Theta = 0.01 = 0.01/(\pi/180)$ deg ≈ 0.6 deg for $\gamma = 0.01$. However, such misorientation is reached after strains that are about one order of magnitude larger. This means that deformation is, in fact, relatively homogeneous on each slip system and that the heterogeneous component is only a small fraction of the total activity. However, this small fraction has important consequences as is apparent from the subgrain structure itself.

The driving force behind the "fragmentation" of the crystal into a "mosaic" of subgrains has long been unclear. However, there is a simple argument for such a driving force. It is related to work hardening. Work hardening results from the interaction of dislocations *via* their stress fields. It is well known that dislocations of the same slip system with the same Burgers vector and the same slip plane interact relatively weakly. The work-hardening coefficient in stage I, where single slip dominates, is relatively small. A high rate of work hardening is found in stage II as soon as secondary slip becomes active. In this stage, the dislocations lie on different mutually intersecting slip planes. They form junctions by recombination and have to intersect their "forest" dislocations during glide. It is this difference in work-hardening rates that is used to explain the organized fragmentation of the crystal into subgranular entities. It will be shown that under these circumstances any disturbance of the homogeneous deformation will grow rather than vanish, thus leading to differences in the change of the shape of the neighboring volume elements. That is, a volume element, which happens to have a predominance of slip on a "primary" system, will deform faster than its surroundings because it contains less dislocation forest. This further stimulates the primary slip activity.

However, the predominance addressed previously would quickly come to an end if the deformation is incompatible. Thus, it is necessary to achieve compatible deformation in the neighboring volume elements. This can be done by appropriate choice of the different primary slip systems in the neighboring regions. By virtue of compatibility, these neighboring regions undergo different lattice rotations, thus constituting subgrains. Then, the dislocations stored at the boundaries of the regions have the character of geometrically necessary dislocations. They constitute subgrain boundaries that, ideally, are without long-range stresses.

As for the size of the subgrains, one has to note that there is a certain extension of the slip zones that decreases with increasing stress. A subgrain is unlikely to be much smaller than this distance, which can be approximated as $100bG/\sigma$ in pure metals. This sets a lower limit to the subgrain size. In fact, the average subgrain size (mean linear intercept) is about $\omega = 23bG/\sigma$. It has to be noted here that three neighboring subgrain boundaries contain dislocations of like sign. Thus, the average spacing of the groups of subgrain boundaries with dislocations of like sign is of the same order of magnitude as the slip line spacing.

The stress dependence means that there is a huge variation of the steady-state subgrain sizes observed in real life, from mm-sized subgrains close to the melting point of pure metals down to 100 nm at the high stresses observed during cold working. However, the fact that a lower limit exists is important for the experimental attempts to produce nanocrystalline materials.

One point is missing in this chain of arguments that is important for the degree of the instability. This is the fact that the subgrains change their crystal orientation with respect to stress. The result is a change in the Schmid factors of the active slip systems. Obviously, the instability, that is the tendency to concentrate slip locally to one system within an arrangement of compatibly deforming subgrains, will increase or decrease depending on whether the Schmid factor of the primary system increases or decreases. The geometrical softening that is related to an increase in Schmid factor will further enhance the instability, *i.e.*, it will lead to further concentration of slip on the primary system. However, with the increasing change in subgrain orientation, the geometrical softening will come to end and turn to geometrical hardening due to decrease of the Schmid factor. This tendency (which is also responsible for the end of stage I work hardening) poses a natural limit to the misorientation to be achieved from a single primary system. From this point of view, it is not possible to reach arbitrary large misorientations by uniaxial deformation. In fact, it has been observed that deformation must follow a certain schedule of passes with different specimen orientations for obtaining large angle boundaries. It is by no means evident that misorientations are continuously increasing during deformation as is reported in many articles on what is called continuous recrystallization.

2. *Quantitative model*

In order to substantiate the qualitative arguments given previously, we look at the simple case of a crystal that is orientated for symmetric double slip. Here, the crystal can choose between two slip systems of the same Schmid factor. Preference of one system leads to a crystal rotation (for compatible deformation) around a common axis. It has been reported by Pantleon and Hansen[1] that the experimentally observed misorientations can be explained on the basis of rotations around two perpendicular axes. This would mean that the real deformation in three dimensions can be obtained from a superposition of compatible subgranular deformation of the type described previously on two sets of symmetric systems with perpendicular rotation axes.

The model of deformation-induced subgrain formation is set up in the framework of classical, continuum crystal plasticity. It rests on the bifurcation analysis of a crystal deforming in plane strain that can be found in the literature in many variants, *e.g.*, References 2 through 7. A detailed step-by-step analysis of a rate-independent, rigid-plastic crystal oriented for symmetric double slip has been presented recently.[8] Here, we are going to review only the main steps of the analysis.

The material velocity field, $\bar{\mathbf{v}} = (\bar{v}_x, \bar{v}_y)$, describing homogeneous deformation of the crystal is disturbed. The perturbation $\hat{\mathbf{v}}(x, y)$ is considered in the form of a planar wave with the wave vector $(k_x, \xi k_x)$ and an infinitesimal amplitude $\tilde{\mathbf{v}}$.

$$\hat{\mathbf{v}}(x, y) = \tilde{\mathbf{v}} \exp i(k_x x + \xi k_x y) \qquad [1]$$

The disturbed deformation fulfills constitutive relations between stress (rate) and strain (rate),

$$\partial_t(\hat{\sigma}_{11} - \hat{\sigma}_{22}) = H_{xx}(\partial_x \hat{v}_x - \partial_y \hat{v}_y) \qquad [2]$$

$$\partial_t \hat{\sigma}_{12} = H_{xy}(\partial_x \hat{v}_y + \partial_y \hat{v}_x)$$

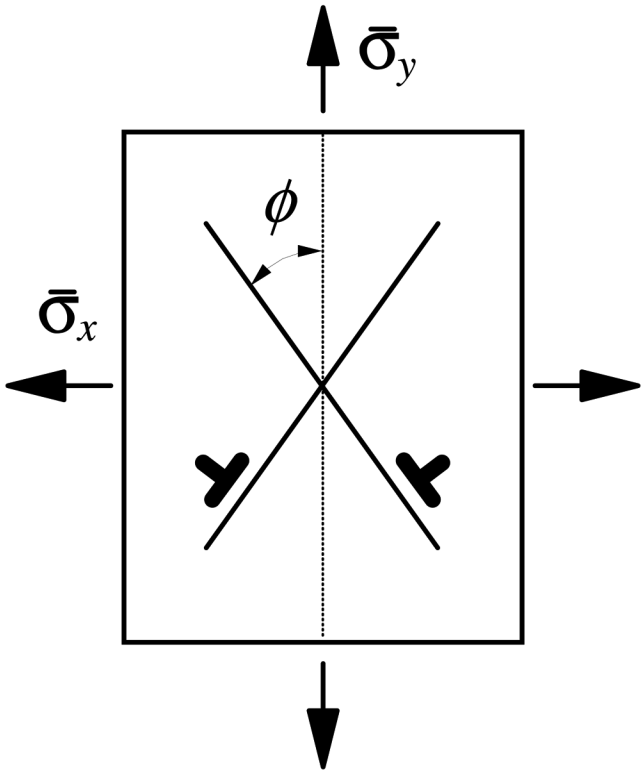

Fig. 1—The symmetric double slip model of a crystal deforming plastically in plane strain.[4] Geometrical axes coincide with the principal directions of the applied stress $\bar{\sigma}$. Without lost of generality, we can assume tension in the *y* and compression in the *x* direction, *cf.* Refs. 2, 8, and 13. The term ϕ is the angle between the tensile axis and the slip direction.

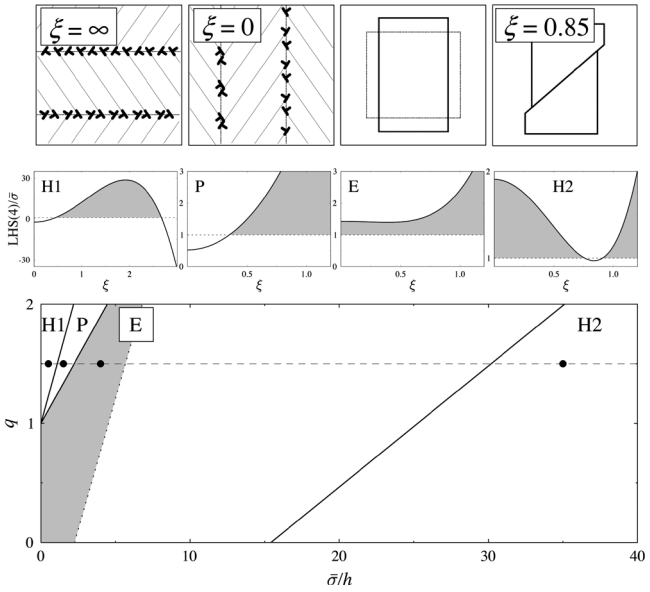

Fig. 2—The bifurcation map corresponding to Eq. [4] is drawn at the bottom of the figure and discussed in the text. The LHS of Eq. [4]/$\bar{\sigma}$-*vs*-ξ diagrams in the middle are computed at the bold dots in the bifurcation map. They are scaled differently to capture the decisive qualitative features of the bifurcation behavior. The sketches at the top symbolize the most unstable bifurcation modes in the corresponding regimes: subgrain boundaries oriented at arctan (ξ) = 90 deg (H1) and arctan (ξ) = 0 deg (P) relative to the tensile axis (*cf.* Fig. 1), homogeneous deformation (*E* below maximum tensile load), and a shear band inclined at arctan (ξ) ≈ 40 deg relative to the tensile axis (H2). The shaded fields help to identify the absence of any instability in the corresponding regimes. The elliptical instability in the form of diffuse necking (*E* above maximum tensile load, no real ξ)[3] is not discussed here.

where $\hat{\sigma}_{ij}$ means a disturbance of the uniform stress field $\bar{\sigma}_{ij}$. The model is termed rate independent, for the flow stress depends only on the current state of the strain not on the strain rate. The instantaneous tangent-hardening coefficients, H_{xy} and H_{xx} (Pa), for shearing parallel to the directions of applied stress and at 45 deg to them, respectively,[3] can be easily interpreted in terms of crystallographic slip,[4,8]

$$H_{xx} = \frac{h(1+q)}{2\sin^2 2\phi}, \quad H_{xy} = \frac{h(1-q) + \bar{\sigma}\cos 2\phi}{2\cos^2 2\phi} \qquad [3]$$

where *h* and *qh* are the usual primary and secondary (latent) hardening coefficients, respectively, and ϕ is the orientation of the slip systems relative to the tensile axis, Figure 1. The difference of the applied axial stress components $\bar{\sigma} = \bar{\sigma}_{yy} - \bar{\sigma}_{xx}$ is assumed to be positive (tension in the *y* and/or compression in the *x* directions). The term $\bar{\sigma}\cos 2\phi$ accounts for the geometrical hardening/softening. The anisotropy of the hardening behavior ($H_{xx} \neq H_{xy}$) is a necessary prerequisite for the appearance of an instability of the homogeneous deformation.

As usual, in the bifurcation analyses, *e.g.*, a buckling instability of a beam,[9] the stress equilibrium is set up at the disturbed (*i.e.*, slightly deformed) system. According to the extension of this concept to continuum, which is due to Biot,[2] the stresses are considered in a system of coordinates x_1Ox_2 that rotates as material fibers do, rather than in the laboratory system *xOy*, *cf.* Eq. [2]. The compatibility of the nonhomogeneous deformation is guaranteed by relating the stress rates in Eq. [2] to the smooth field of material velocities in Eq. [1]. By accounting also for the incompressibility (volume constancy) of the plastic deformation, one finally arrives at the characteristic equation:

$$\left(H_{xy} + \frac{1}{2}\bar{\sigma}\right)\xi^4 + 2(2H_{xx} - H_{xy})\xi^2 + \left(H_{xy} + \frac{1}{2}\bar{\sigma}\right) = \bar{\sigma} \qquad [4]$$

The appearance of instability is related to the existence of a positive root ξ^2 of Eq. [4], *i.e.*, to the loss of ellipticity of the corresponding governing differential equation.[3] A positive root appears (and an instability occurs) if the secondary hardening is strong enough ($q > 1$) and/or the geometrical softening appears ($\bar{\sigma}\cos 2\phi < 0$), *cf.* Eq. [3]. For the roots, ξ, the left-hand side (LHS) of Eq. [4] takes the meaning of the critical (bifurcation) stress. The instability is possible for all ξs for which the inequality LHS [4] $< \bar{\sigma}$ is verified. The most unstable bifurcation mode displays the greatest difference $\bar{\sigma}$ − LHS [4].

The stability behavior resulting from the analysis of Eq. [4] is summarized in Figure 2, showing (a) the bifurcation map in the lower part, (b) the corresponding LHS [4]-*vs*-ξ diagrams in the middle, and (c) sketches symbolizing the most unstable deformation modes (if any) in the upper part of the figure. The case considered is representative of an fcc crystal oriented for symmetric double slip in tension:[4,10] the inclination of slip planes to tensile axis ϕ = 35 deg, Figure 1. The abscissa of the bifurcation map reflects the effect of geometrical hardening/softening, and the ordinate the effect of secondary hardening. An instability can occur in the hyperbolic (H1, H2), parabolic (P), or even elliptic (E) regime beyond the maximum tensile load (dotted line).

Simplifying, one may say that the strong latent hardening is the main cause for the formation of misorientations in the course of hardening where the macroscopic deformation is still nominally homogeneous, while the geometrical softening is mainly responsible for localization into shear bands (macroscopically nonhomogeneous deformation) when the hardening coefficient becomes sufficiently small relative to the applied stress.[3–5,8] Suppose, for example, the ratio latent-to-active hardening $q = 1.5$. The tensile test starts in the H1 regime, which means the instability responsible for lattice misorientations is possible from the onset. With the growing applied stress, $\overline{\sigma}$, and falling hardening modulus, h, we move across the P field into the E one, where the stabilizing impact of geometrical hardening overwhelms the destabilizing effect of secondary hardening, until the maximum tensile load is reached and geometrical softening takes the upper hand, causing diffuse necking (elliptical instability).[3] Finally, localization of deformation takes places in the H2 regime where the geometrical softening dominates. Note the ξs that dominate the particular regimes: $\xi = \infty$ in H1, $\xi = 0$ in P, and $\xi = 0.85$ in H2. As discussed previously, they are determined by the smallest ratio LHS [4]/$\overline{\sigma} < 1$. These ξs determine the characteristic direction arctan (ξ) of the instability in the general form of Eq. [1] and, thus, govern the appearance of resulting dislocation patterns H1 and P, respectively, and the direction of the band of localized deformation, H2. In view of the fact that ξ changes abruptly at the border between H1 and P, it is difficult to tell on the grounds of the present stability analysis alone which one (if any) would dominate the dislocation pattern in reality.

The dislocation patterns associated with the instability are determined by the dislocation density tensor,[11,12] which is directly related to the lattice rotations accompanying the instability. The diffuse dislocation patterns derived from the velocity field (Eq. [1]) represent embryonic stages of subgrain formation.[13,8] It is expected that volume elements of a common misorientation surrounded by well-defined boundaries will develop in the postbifurcation regime from the continuously distributed misorientations and dislocation patterns predicted by the present linear-stability analysis. This expectation is visualized in Figure 2 (H1, P), which shows dislocation boundaries constructed at the crests of the computed continuous dislocation density waves. For more details, see References 8 and 13.

B. *Climb-Glide*

1. *Qualitative arguments*

In the preceding rate-independent model of crystal plasticity, the effect of strain rate on the flow stress is neglected. This approximation turns out to be applicable to pure metals where the work hardening dominates the plastic response. However, in strongly solute-hardened alloys under creep conditions where dislocations with solute atmospheres move slowly in a viscous manner,[14] the work hardening can be neglected, while the hardening due to strain rate becomes essential. In these so-called noncell forming materials, deformation-induced subgrain structures form at larger strains compared to pure metals.[15,16] Anyway, their origin can be explained as a mechanical instability as well. The decisive role in the corresponding model is played by climb of dislocations.[17] The climb velocity is comparable with the velocity of the viscous glide: both of them are diffusion-controlled.[18,14,13] The resolved climb-deformation rate is understood as being proportional to the rate of change of the area of the inserted atomic planes per unit volume caused by climbing dislocations of the i-th slip system. Assuming for simplicity that there are no sinks for vacancies in the perfect, infinitely extended single crystal considered, the climb deformation can proceed only by exchange of vacancies between dislocations: the vacancies emitted by climbing dislocations of one slip system are absorbed by dislocations of the other slip system. Such a climb deformation does not contribute to the homogeneous deformation in the symmetric double slip model. In reality, the surface of the crystal or grain boundaries can serve as sinks for vacancies, so that a net deformation by climb occurs. This possibility is not considered here to avoid introduction of complicated boundary conditions, *etc.* Only the net deformation by climb, due to exchange of vacancies between dislocations that sets in locally as soon as there is a disturbance of the symmetry, is decisive for the present model.[13,19] This mechanism opens up an additional possibility for local plastic shearing (Figure 3). If it is energetically advantageous, it is taken up by the crystal, which results in a nonhomogeneous plastic flow. The fragmentation of the crystal is, then again, a consequence of the compatibility requirement posed on the disturbed deformation.

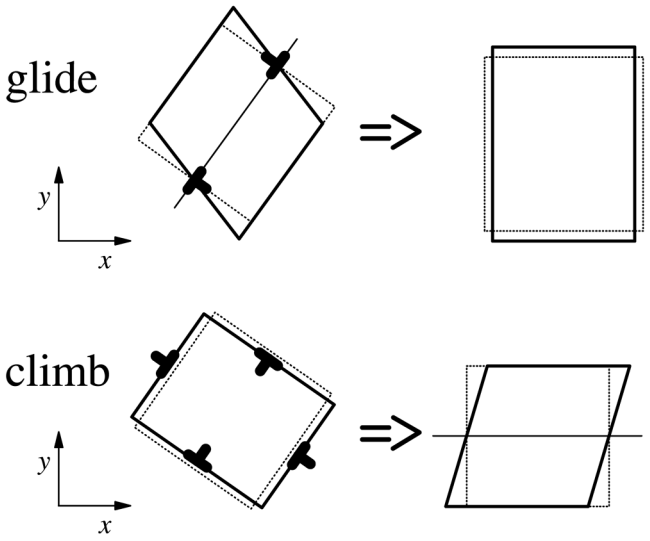

Fig. 3—The role played by glide and climb in a local deformation of a volume element. To separate the effects of glide and climb, the inclination of glide planes to the tensile axis $\phi = 45$ deg is considered (Fig. 1). Then, climb results in shearing parallel to the directions of applied stress, glide in shearing at 45 deg to them (*i.e.*, axial deformation in symmetric double slip; *cf.* also the role of the hardening coefficients in the constitutive Eq. [2]).

For the proposed model to work, it is necessary that glide and climb contribution to the extra nonhomogeneous deformation (perturbation of the homogeneous flow) be comparable. Admittedly, it is difficult to believe that the *deformation* by climb could be so effective that its contribution could be comparable in magnitude with that of glide, even in strongly solute-hardened alloys at low stresses and high temperatures.* Let us recall in this context an alternative to our approach, *viz.* an earlier work on the effect of nonSchmid stresses on stability of plastic flow.[20] In this rate-independent model, stability of plastic deformation by single slip

*L. Kubin: private communication, CNRS/ONERA, France, 1999.

was investigated. Obviously, an instability due to secondary hardening, *cf.* Section II–A, is excluded in such a situation. Therefore, one expects an instability not to appear before the hardening coefficient falls to zero or even becomes negative (softening), *cf.* the field H2 in Figure 2. However, it was found that an instability in the course of hardening (positive hardening coefficient) is possible if the shear strain rate depends not only on the resolved shear stress, but also on other ("non-Schmid") stress components. The proposed physical interpretation is that certain non-Schmid stresses drive cross-slip, which enables gliding dislocations to bypass local obstacles in the slip plane. Note that no net contribution of cross-slip to *deformation* was considered. Turning back to our problem, we see that such an interpretation would be in accord with the traditional role of climb in creep theories: deformation is due to glide, climb enables bypassing of obstacles.[21] It could be worthwhile to pursue this alternative explanation of the subgrain formation in noncell forming materials as well. Here, we return to the preceding model, which assumes comparable glide and climb contributions to the disturbed extra deformation.

2. *Quantitative model*

The model is an extension of the standard crystal plasticity. It was originally sketched by Kratochvíl and Orlová[17] as a direct application of Biot's deformation-induced internal-buckling instability in anisotropic viscous flow,[22,2] then adopted into the framework of symmetric double slip and treated as a complementary model to the preceding rate-independent one.[13,19]

In this model, the plastic deformation is treated as a viscous flow. The infinitesimal amplitude $\tilde{\mathbf{v}}$ of the disturbance (Eq. [1]) is considered explicitly time dependent:

$$\tilde{\mathbf{v}}(t) = \check{\mathbf{v}} \exp(\omega t) \qquad [5]$$

The strain hardening of the rate-independent model, Section II–A, is replaced by strain-rate hardening. Constitutive equations relate stress to strain rate:

$$\begin{aligned} \hat{\sigma}_{11} - \hat{\sigma}_{22} &= \mu_{xx}(\partial_x \hat{v}_x - \partial_y \hat{v}_y) \\ \hat{\sigma}_{12} &= \mu_{xy}(\partial_x \hat{v}_y + \partial_y \hat{v}_x) \end{aligned} \qquad [6]$$

The instantaneous tangent viscosity coefficients μ_{xy} and μ_{xx} (Pa s) for shearing parallel to the directions of applied stress and at 45 deg to them, respectively, can be interpreted in terms of crystallographic glide and climb.[13,19]

$$\begin{aligned} \mu_{xx} &= \frac{\mu_G}{2 \sin^2 2\phi}, \\ \mu_{xy} &= \frac{\mu_G \mu_C}{2(\mu_C \cos^2 2\phi + \mu_G \sin^2 2\phi)} \left(1 + \frac{\overline{\sigma} \cos 2\phi}{\omega \mu_G}\right) \end{aligned} \qquad [7]$$

The crystallographic glide and climb viscosity coefficients μ_G and μ_C relate the resolved shear stress to the shear strain rate and the climb-driving stress to the net strain rate caused by climb, respectively.[13,19] The climb-driving stress has been proposed in Reference 13 by requiring that applied stress, $\overline{\sigma}$ be work-conjugate to overall strain rate, $\dot{\varepsilon}$. One notes that climb provides the anisotropy ($\mu_{xx} \neq \mu_{xy}$), which is necessary for the instability to appear. This is best seen by considering the case of $\phi = 45$ deg: then $\mu_{xx} = \mu_G/2$ and $\mu_{xy} = \mu_C/2$, *cf.* Figure 3. In this special case, only the climb deformation can cause shearing parallel to the directions of applied stress, *cf.* Eq. [6].

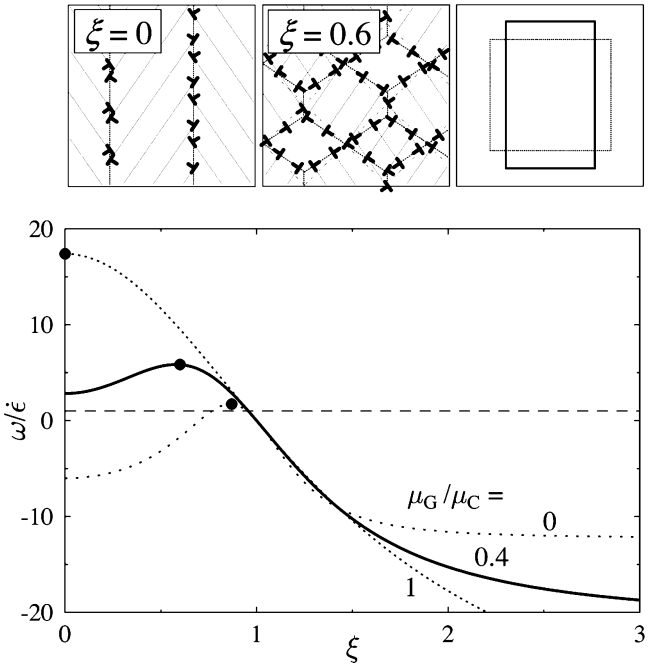

Fig. 4—Stability diagram corresponding to Eq. [8] for different ratios between climb and glide viscosity coefficients (bottom). Dislocation patterns corresponding to the instabilities ($\mu_g/\mu_c = 1$ and 0.4) are computed in the bold dots of the stability diagram ($\xi = 0$ and 0.6) (top). Since the tendency to instability is insignificant for $\mu_g/\mu_c = 0$, homogeneous deformation is symbolically shown in this case. See the text for details.

The term in parenthesis in Eq. [7] accounts for the geometrical softening/hardening, which play the same role as in the rate-independent model. By considering the incompressibility of plastic deformation and stress equilibrium formulated on the disturbed system,[2] one finally arrives at an implicit eigenvalue equation for the amplification factor, ω:

$$\left(\omega\mu_{xy} + \frac{1}{2}\overline{\sigma}\right)\xi^4 + 2\omega(2\mu_{xx} - \mu_{xy})\xi^2 + \left(\omega\mu_{xy} + \frac{1}{2}\overline{\sigma}\right) = \overline{\sigma} \qquad [8]$$

The aim of the stability analysis is to find ω as a function of the material properties and of the ratio of wavelengths, ξ, of the disturbance (Eq. [5]). The homogeneous deformation is stable only if $\omega < 0$, that is if any perturbation (Eq. [5]) dies down. In the other case ($\omega > 0$), the perturbation grows, the homogeneous deformation is unstable, and a kind of deformation-induced structure appears. One should note for completeness that the instability is significant only if the amplification factor is much greater than the rate of homogeneous deformation, $\omega \gg \dot{\varepsilon}$. In such a case, the medium can be treated as being initially at rest rather than in the state of steady flow.[2] This is what we have done here. The dependence of $\omega/\dot{\varepsilon}$ on ξ resulting from Eq. [8] for ratio $\mu_G/\mu_C \approx 0.4$ (glide slightly easier than climb) representing Al 5 pct Mg deformed at 30 MPa/573 K[13] is plotted in Figure 4. The most unstable solution is the one possessing the maximum positive ω. It corresponds to $\xi \approx 0.6$. The dislocation pattern in the form of closed subgrains is constructed from the disturbance (Eq. [1]) *via* the dislocation

density tensor as described in Section II–A and shown in the upper part of Figure 4.

To demonstrate the destabilizing effect of climb, the diagram in Figure 4 is completed by the $\omega/\dot{\varepsilon}$ dependence on ξ for ratios $\mu_G/\mu_C = 1$ (climb as easy as glide) and $\mu_G/\mu_C = 0$ (no climb at all). In the former case, the instability is substantially stronger and the dominant ξ shifts towards 0. In the latter case, the instability is insignificant, the deformation remains homogeneous (strictly speaking, the stability analysis in the present simple form is not applicable). If in addition to the absence of climb the orientation $\phi = 45$ deg is considered, even the tendency to instability would disappear, *cf.* Figure 3 and the corresponding discussion.

III. CONSEQUENCES OF SUBGRAIN FORMATION

A. *Long-Range Internal Stresses*

1. *Qualitative arguments*

Studies of X-ray line broadening have shown that cell walls with high dipole content whose thickness is far larger than the average boundary dislocation spacing are associated with long-range internal stresses.[23,24] To explain the internal stresses of cell boundaries, it is possible to treat them as plastically hard regions of a composite-like material, the soft phase of which is presented by the cell interiors.[25] Compatibility of the material (elastic plus plastic) deformation requires that the misfit of plastic strain between the two phases, which is accommodated by dislocation segments deposited at the interfaces between the cell boundaries and interiors, be compensated by elastic deformation, which is enforced by the long-range internal stresses.[25] Predictions of the one-dimensional (1-D) composite model have been verified by 2-D dislocation mechanics calculations,[26,27] as well as by 2-D continuum-mechanics numerical calculations.[28]

As argued previously, ideal subgrains are free from long-range internal stresses as the underlying plastic deformation accompanied by stress-free lattice rotation is compatible, in other words, the parts of the "mosaic structure" fit perfectly together. However, studies of X-ray line broadening have shown that there is only little quantitative change concerning the internal stresses if one goes from a dislocation cell structure towards a subgrain structure in pure Cu, by increasing the temperature of deformation at the same stress.[29,30] We note that the sensitivity of the X-ray technique is not sufficient at low stresses. However, the complementary method of observing bowed dislocation segments at subgrain boundaries verifies the existence of high forward stresses at the boundaries even for high temperatures and relatively low stresses.[31,32] Another result of the X-ray line broadening studies is a small reduction of the volume fraction of subgrain boundaries compared to thick cell walls.[29,30] This is puzzling, as a subgrain boundary has a width (spacing up to which the stress field of an ideal boundary extends in the direction perpendicular to the boundary) that is in the order of the dislocation spacing in the boundaries. Thus, the volume fraction of ideal subgrain boundaries should be almost negligible and also the explanation of internal stresses in terms of dislocation segments deposited at the interfaces[25] makes no sense, as it is inconsistent with the well-established picture of subgrain boundary as a 2-D dislocation network.[31,32]

A solution to the puzzle is that it is not only the deposition of dislocation segments at the boundaries that creates the internal stresses. During plastic deformation, gliding dislocations have to bow between the boundaries that act as obstacles to their motion. As a consequence, there is a deficit of plastic strain near the boundaries that has to be compensated elastically, *cf.* Reference 33. In this way, internal forward stresses in the vicinity and at the boundaries are created. Quantitatively, this mechanism contributes moderately to the internal stresses in cell structures,[34] but it seems to be dominant in subgrain structures.[35] It also explains the continuous internal-stress profile with a maximum at the boundaries found by evaluating the dislocation curvature in both cells and subgrains.[25,31–33] It follows that the effective width of the region with internal forward stresses is distinctly larger than the boundary region itself. It is the former and not the latter that determines the volume fraction of a "hard" region entering the interpretation of X-ray results in terms of the composite model.[23,24,29,30] From this description, it is also clear that the maximum internal forward stress at the thin subgrain boundary itself is distinctly larger than the average internal forward stress resulting from the classical version of composite model, which assumes a constant value of internal forward stress in the hard region.[25]

The role played by the internal stresses in the plastic response of the crept material is twofold: (a) the internal back stresses in subgrain interiors cause kinematic hardening, *cf.* References 36, which is responsible for the decrease of creep rate in the extended primary stage of creep of pure materials where the density of free dislocations is apparently constant, and (b) the internal forward stresses at subgrain boundaries enable their intersecting by free dislocations in spite of the small "forest dislocation" spacing in the boundaries.

2. *Quantitative model*

Implementation of the preceding ideas in a static model of long-range internal stresses is easy. One can simply assume the gliding dislocations take up a curved configuration, *e.g.*, an elliptical one, in accord with TEM observations.[33] This causes an elliptic profile of plastic deformation in the subgrains.

Then, upon considering stress equilibrium, strain compatibility, and Hooke's law, one computes the internal stresses. This has been done analytically in the composite model framework,[33,34] as well as numerically in the full continuum mechanics formulation in two dimensions[37] with qualitatively similar results. However, the 2-D formulation[37] has revealed a strong dependence of the magnitude of internal stresses on the relative orientation of glide planes and subgrain boundaries, an effect that cannot be accounted for in the 1-D framework[25,33] and that deserves further pursuit.

Anyway, the composite-model framework[25] appears to be a suitable basis for further development of the model, especially because it allows for analytical solutions. In this 1-D isostrain approximation to continuum mechanics, one requires not only compatibility, but even homogeneity of material (elastic + plastic) shear strain,

$$\overline{\gamma} = \gamma^e(x) + \gamma^P(x) \qquad [9]$$

On the other hand, one relaxes stress equilibrium by allowing

for nonhomogeneous shear stress, thus enabling the existence of internal stresses. Stress equilibrium is fulfilled on average (Abenga's law[12,38]), requiring that nonhomogeneous shear stress averaged over a period consisting of a soft subgrain interior, s, and hard boundary, h, equals the applied shear stress,

$$\frac{1}{s+h}\int_{\langle s+h\rangle}\tau(x)dx = \bar{\tau} \qquad [10]$$

Increment of plastic shear caused by the displacement, $\varphi(x)$, of the mobile dislocations with density, ρ_m, and Burgers vector magnitude, b, follows from the Orowan equation,

$$\gamma^P(x) = \rho_m b\varphi(x) \qquad [11]$$

In the following, rather than assuming the elliptical shape of the bowing dislocations,[33] we compute it by considering the equilibrium of forces acting on them: (ii) the Peach–Koehler force due to the local shear stress, $\tau(x)$, and (b) the self force due to (constant) line tension $T \approx Gb^2$. The equilibrium position of a bowing screw dislocation fulfills relation

$$\tau(x)b + T\partial_x^2\,\varphi(x) = 0 \qquad [12]$$

The second derivative of the dislocation displacement, $\varphi(x)$, follows from linearized dislocation curvature, cf. Reference 39. Strictly speaking, the linearized model correctly describes only mild bowing of dislocations between the subgrain boundaries (anelasticity). The full-curvature model using parametric description of dislocation lines,[40] which is appropriate for plasticity, has been set up, solved numerically, and compared with the linearized one in Reference 41. The comparison has revealed remarkably satisfying distribution of internal stresses resulting from the linearized model, especially if no deposition of dislocation segments at the interfaces is possible (as in the case of subgrain boundaries). Analytical solution of the linearized problem, Eqs. [9] to [12], can be found by considering Hooke's law for the elastic shear strain, $\gamma^e(x) = \tau(x)/G$, and suitable boundary conditions.[42,43,41] Stresses at the subgrain boundary, τ_h, and in subgrain interior, τ_s, result in

$$\tau_h = \frac{\bar{\tau}(s+h)\cosh\left(\frac{s}{2}\sqrt{\rho_m}\right)}{\frac{2}{\sqrt{\rho_m}}\sinh\left(\frac{s}{2}\sqrt{\rho_m}\right) + h\cosh\left(\frac{s}{2}\sqrt{\rho_m}\right)},$$
$$\tau_s(x) = \frac{\tau_h\cosh\left(x\sqrt{\rho_m}\right)}{\cosh\left(\frac{s}{2}\sqrt{\rho_m}\right)} \qquad [13]$$

Clearly, the stress in subgrains, $\tau_s(x)$, increases continuously from the interior to the boundary, where it reaches its maximum value, $\tau_s(\pm s/2) = \tau_h$. The reduced shear-stress profile, $\tau_s(x)/\bar{\tau}$, is plotted in the rightmost diagram of Figure 5 for the volume fraction of subgrain boundaries, $f_h = h/(s+h) = 0.01$. The subgrain size has been estimated as $s = 20bG/\bar{\sigma}$, and the spacing of mobile dislocations as $1/\sqrt{\rho_m} = bG/\bar{\sigma}$. Model material parameters have been taken over from Reference 41. One recognizes that the volume fraction of material experiencing forward internal stress is about $f \approx 0.23 \gg 0.01$ and that the forward stress at the boundary itself is much greater than the applied stress, $\tau_h/\bar{\tau} \approx 9 \gg 1$. We note that the classical composite model[25] gives, in the present case, the volume fraction $f = f_h = 0.01$ and stress concentration at the boundary,* $\tau_h/\bar{\tau} = 100$.

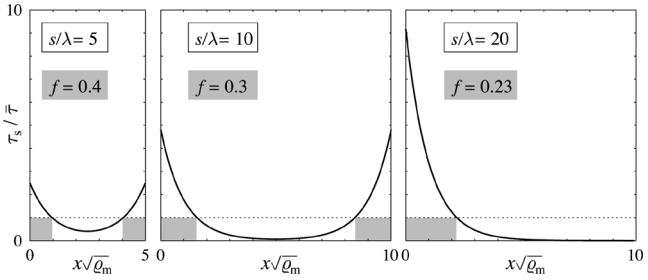

Fig. 5—Size dependence of subgrain hardening is demonstrated by plotting the reduced stress profiles in subgrains for various ratios s/λ. The rightmost diagram corresponds to steady-state deformation ($s\sqrt{\rho_m} \approx 20$). Here, the dislocations bow relatively easily, so the stress in the subgrain interior could decrease to the local flow stress (which is assumed to be zero for simplicity). In the other cases, the flexibility of the dislocations bowing in the small subgrains determines the response. One notes the volume fraction f of the material under forward internal stress (shaded). The classical composite model[25] reappears at $s/\lambda = \infty$, resulting in $f = 0.01$ and the reduced stress $\tau_s/\bar{\tau}$ changing abruptly at the boundary from 0 in the subgrain to 100 at the boundary; see the text for details.

*The athermal stress due to dislocation interactions that would normally be $\tau_{G,\rho} \propto bG\sqrt{\rho_m}$ and that would reduce the stress concentration by virtue of the rule of mixtures $\bar{\tau} = (1 - f_h)\tau_{G,\rho} + f_h\tau_h$ has been neglected here for simplicity.

B. *Size Dependence of Subgrain Hardening*

1. *Qualitative arguments*

The kinematic hardening due to long-range internal stresses discussed in Section III–A is subgrain-size dependent. This can be seen, for example, in creep of ferritic steels that inherit fine subgrain structure stemming from the strong internal deformation related to the martensitic transformation in the course of production. In the tertiary stage of creep after the minimum of creep rate, most of the microstructure parameters are practically saturated, but the subgrains (and carbides) still grow while the steel softens.[44,45] In general, the size dependence of flow stress on subgrain size is reflected by the empirical expression for the stress dependence of subgrain size, $w \propto bG/\sigma$.

These findings are in accord with the motto of the generalized, Cosserat, or strain-gradient plasticity theories: "smaller is stronger."[46–49] Among other things, these theories aim at describing the influence of grain size on hardening and flow stress.[50,51] While the formal description succeeds, and the experimentally observed size effect is usually correctly reflected, the proposed physical interpretation in terms of isotropic hardening due to the storage of geometrically necessary dislocations is often questionable. For example, it is well known that the precipitation hardening in $\gamma - \gamma'$ nickel-based superalloys is due to the bowing of glide dislocations in the soft narrow channels (Orowan stress, kinematic hardening). When modeled by a strain-gradient plasticity theory, the hardening is related to the storage of geometrically necessary dislocations in the channels (isotropic hardening). So it is true that: "Although dislocation-based arguments are used as motivation, these theories are phenomenological."[52]

Such discrepancies motivate us to propose a simple Cosserat theory that is able to account for the size-dependent kinematic hardening caused by the bowing of dislocations between subgrain boundaries (or even γ' precipitates). Let us note that the model of long-range internal stresses presented in Section III–A is in fact nonlocal: the self-energy (line tension) of dislocations bowing between the plastically hard phase introduces a length scale into the continuum mechanics description. The model can be related directly to the Cosserat model proposed in Reference 41. In doing so, the Cosserat intrinsic length scale, Cosserat rotation, and the corresponding higher order boundary conditions acquire a concrete physical interpretation. Let us note that in strain gradient plasticity theories, the intrinsic length is usually obtained by a fitting procedure.[46] Physical interpretation of higher-order boundary conditions in generalized plasticity is in general difficult and a subject of ongoing discussion.[48,49,52]

2. *Quantitative model*

In the 1-D composite model, the shear strain $\gamma(x)$, Eq. [9], reflects the translational degree of freedom of classical continuum. Cosserat continuum possesses an additional independent-rotational degree of freedom, represented by rotation $\Phi(x)$. As a consequence, the stress tensor is no more symmetric and a couple stress appears, which is related to Cosserat curvature $\partial_x\Phi(x)$ by an intrinsic length λ (m). This renders the theory nonlocal, thus enabling it to account for size effects.[47,41]

Let us treat subgrain interior as a 1-D elastic Cosserat continuum, while subgrain boundaries remain classically elastic. We still require the homogeneity of material shear (Eq. [9]). As shown in Reference [41], one is able to formulate a governing equation for the Cosserat rotation,

$$\lambda^2\partial_x^2\,\Phi - \Phi = 0 \qquad [14]$$

This equation can be identified with an equation for lattice rotation $\Phi = -\gamma^e/2$, which results from the dislocation model presented in Section III–A, while the Cosserat intrinsic length appears to correspond to the mean spacing between mobile dislocations, $\gamma = 1/\sqrt{\rho_m}$,[41]. The size dependence of the dislocation model is, thus, reflected by the ratio between the characteristic length of deformation field (here the subgrain size $s = w$) and the intrinsic length, λ (here the spacing between mobile dislocations*), $s\sqrt{\rho_m} = s/\lambda$ in Eq. [13].

*We note that in the proposed interpretation, the intrinsic length is no material parameter, but it varies in the course of plastic deformation as the dislocation density does.

Figure 5 shows the size dependence of the computed stress profiles for three different ratios, s/λ. The natural physical interpretation is that the Orowan bowing of gliding dislocations is more difficult in the small subgrains than in large ones. Since the stress profiles in subgrains $\tau_s(x)$ are directly related to the shape of bowing dislocations, *cf.* Eqs. [11] and [9], one can see this effect directly in Figure 5. Without line tension or in infinitely large subgrains, the dislocation model reduces to the classical composite model,[25] and the size effect disappears.[41]

Within the preceding identification, the boundary conditions for the Cosserat rotation, *i.e.*, the higher-order boundary conditions, take the meaning of a requirement for continuity of lattice rotation at the interfaces,

$$\Phi\left(\pm\frac{s}{2}\right) = -\frac{\tau_h}{2G} \qquad [15]$$

From the lattice rotation resulting from Eq. [14] with boundary conditions (Eq. [15]), a density of geometrically necessary dislocations (corresponding equivalently to the plastic strain gradient, *cf.* Eq. [11]) results.[41] As distinct from the conventional strain-gradient plasticity theories, these dislocations are not assumed to contribute to isotropic hardening, at least in the present single slip model, *cf.* Reference [53].

We conclude that the size-dependent (kinematic) subgrain hardening can be accounted for equivalently—at least in the simplifying 1-D composite model framework—either by the dislocation model of Section III–A or by the preceding Cosserat model.[41] The relation between the two approaches is a subject of ongoing investigation. It can shed some light upon some open questions of nonlocal plasticity theories (interpretation of intrinsic length, physical relevance of higher order boundary conditions, *etc.*).

IV. CONCLUSIONS

The formation of subgrain structures in the course of nominally uniform plastic deformation has been explained as a mechanical instability of the type of internal bending. In pure materials, the physical origin of the instability is secondary hardening, which is stronger than the primary one. In strongly solid-solution hardened alloys, the climb of dislocations plays the destabilizing role. Additionally, the stability behavior is in both cases influenced by geometrical effects (changing of Schmid factor), which are mainly responsible for localization in the later stages of deformation.

The subgrain boundaries formed present obstacles to the motion of gliding dislocations, which are, thus, forced to take a bowed configuration. As a consequence, long-range internal back stresses arise in the subgrains and forward stresses at the boundaries. The former lead to kinematic hardening, the latter enable the dislocations to penetrate the boundaries. It is more difficult for the dislocations to squeeze through small subgrains than through large ones, which results in size-effect in the subgrain hardening: smaller subgrains are harder. This behavior can be alternatively described by a generalized plasticity model with boundary conditions for lattice rotation (higher order boundary conditions).

A natural next step in the development of the present ideas is a combination of the model for subgrain formation with the model of size-dependent subgrain hardening to get a model predicting the size of the forming subgrains.

REFERENCES

1. W. Pantleon and N. Hansen: *Acta Mater.*, 2001, vol. 49, pp. 1479-93.
2. M.A. Biot: *Mechanics of Incremental Deformations*, John Wiley, New York, NY, 1965.
3. R. Hill and J.W. Hutchinson: *J. Mech. Phys. Solids*, 1975, vol. 23, pp. 239-64.
4. R.J. Asaro: *Acta Metal.*, 1979, vol. 27, pp. 445-53.
5. D. Peirce, R.J. Asaro, and A. Needleman: *Acta Metall.*, 1982, vol. 30, pp. 1087-1119.
6. H.M. Zbib and E.C. Aifantis: *Res. Mech.*, 1988, vol. 23, pp. 261-77.
7. J. Kratochvíl: *Scripta Metall. Mater.*, 1990, vol. 24, pp. 1225-28.
8. R. Sedláček, J. Kratochvíl, and W. Blum: *Phys. Status Solidi (a)*, 2001, vol. 186, pp. 1-16.

9. P. Timoshenko and J.M. Gere: *Theory of Elastic Stability*, 2nd ed., McGraw-Hill, New York, NY, 1963.
10. R.J. Asaro and A. Needleman: *Scripta Metall.*, 1984, vol. 18, pp. 429-35 (Viewpoint set No. 6).
11. J.F. Nye: *Acta Metall.* 1953, vol. 1, pp. 153-62.
12. E. Kröner: *Kontinuumstheorie der Versetzungen und Eigenspannungen*, Springer, Berlin, 1958.
13. R. Sedláček: Ph.D. Thesis, Universität Erlangen-Nürnberg, Erlangen, Mar. 2000.
14. T. Endo, T. Shimada, and T.G. Langdon: *Acta Metall.*, 1984, vol. 32, pp. 1991-99.
15. D.A. Hughes: *Acta Metall. Mater.*, 1993, vol. 41, pp. 1421-30.
16. W. Blum, C. Schlögl, and M. Meier: *Z. Metallkd.*, 1995, vol. 86, pp. 631-37.
17. J. Kratochvíl and A. Orlová: *Phil. Mag.*, 1990, vol. A61, pp. 281-90.
18. J. Weertman: *Phil. Mag.*, 1965, vol. 11, pp. 1217-23.
19. R. Sedláček, J. Kratochvíl, and W. Blum: *Deformation-Induced Microstructures: Analysis and Relation to Properties*, Proc. 20th Risø Int. Symp. on Materials Science, J.B. Bilde-Sørensen, J.V. Carstensen, N. Hansen, D. Juul Jensen, T. Leffers, W. Pantleon, O.B. Pedersen, and G. Winther, eds., Risø National Laboratory, Roskilde, Denmark, 1999, pp. 487-92.
20. R.J. Asaro and J.R. Rice: *J. Mech. Phys. Solids*, 1977, vol. 25, pp. 309-38.
21. J. Weertman: *Trans. ASM*, 1968, vol. 61, pp. 681-94 (no copy).
22. M.A. Biot: *J. Franklin Inst.*, 1965, vol. 279, pp. 65-82.
23. T. Ungár, H. Mughrabi, D. Rönnpagel, and M. Wilkens: *Acta Metall.*, 1984, vol. 32, pp. 333-42.
24. H. Mughrabi, T. Ungár, W. Kienle, and M. Wilkens: *Phil. Mag.*, 1986, vol. A53, pp. 793-813.
25. H. Mughrabi: *Acta Metall.*, 1983, vol. 31, pp. 1367-79.
26. M. Hecker and H.J. Burmeister: *Phys. Status Solidi (a)*, 1996, vol. 158, pp. 87-100.
27. R. Sedláček: *Comput. Mater. Sci.*, 1996, vol. 7, pp. 21-26.
28. R. Sedláček and M. Hecker: *Comput. Mater. Sci.*, 1998, vol. 11, pp. 270-76.
29. S. Straub, W. Blum, H.J. Maier, T. Ungár, A. Borbély, and H. Renner: *Acta Mater.*, 1996, vol. 44, pp. 4337-50.
30. A. Borbély, W. Blum, and T. Ungár: *Mater. Sci. Eng. A*, 2000, vol. 276, pp. 186-94.
31. M.A. Morris and J.L. Martin: *Acta Metall.*, 1984, vol. 32, pp. 549-61.
32. M.A. Morris and J.L. Martin: *Acta Metall.*, 1984, vol. 32, pp. 1609-23.
33. H. Mughrabi: *Phys. Status Solidi (a)*, 1987, vol. 104, pp. 107-20.
34. R. Sedláček: *Scripta Metall. Mater.*, 1995, vol. 33, pp. 283-88.
35. R. Sedláček, S. Straub, A. Borbély, T. Ungár, and W. Blum: *Key Eng. Mater.*, 1995, vols. 97–98, pp. 461-66.
36. R.J. Asaro: *Acta Metall.*, 1975, vol. 23, pp. 1255-65.
37. R. Sedláček and W. Blum: *Comput. Mater. Sci.*, 1998, vol. 13, pp. 148-53.
38. T. Mura: *Micromechanics of Defects in Solids*, Martinus Nijhoff Publishers, Dordrecht, 1982.
39. J. Kratochvíl and M. Saxlová: *Scripta Metall. Mater.*, 1992, vol. 26, pp. 113-16.
40. R. Sedláček: *Phil. Mag. Lett.*, 1997, vol. 76, pp. 275-80.
41. R. Sedláček and S. Forest: *Phys. Status Solidi (b)*, 2000, vol. 221, pp. 583-96.
42. R. Sedláček: *Key Eng. Mater.*, 1995, vols. 97–98, pp. 497-500.
43. R. Sedláček: *Phys. Status Solidi (a)*, 1995, vol. 149, pp. 85-93.
44. W. Blum, S. Straub, and S. Vogler: *High Temp. Mater. Processes*, 1993, vol. 12, pp. 31-47.
45. M. Meier and W. Blum: *Mater. Sci. Eng., A* 1993, vol. 164, pp. 290-94.
46. N.A. Fleck, G.M. Muller, M.F. Ashby, and J.W. Hutchinson: *Acta Metall. Mater.*, 1994, vol. 42, pp. 475-87.
47. S. Forest, G. Cailletaud, and R. Sievert. *Arch. Mech.*, 1997, vol. 49, pp. 705-36.
48. A. Needleman: *Acta Mater.*, 2000, vol. 48, pp. 105-24.
49. J.W. Hutchinson: *Int. J. Solids Struct.*, 2000, vol. 37, pp. 225-38.
50. V.P. Smyshlyaev and N.A. Fleck: *J. Mech. Phys. Solids*, 1996, vol. 44, pp. 465-95.
51. S. Forest, F. Barbe, and G. Cailletaud: *Int. J. Solids Struct.*, 2000, vol. 37, pp. 7105-26.
52. A. Needleman and E. Van der Giessen: *Mater. Sci. Eng. A*, 2001, vols. 309–310, pp. 1-13.
53. H. Mughrabi: *Proc. TMS Symp. in Honor of Ali Argon*, San Diego, CA, Mar. 1999; *Mater. Sci. Eng. A.*, 2001, vol. 317, pp. 171–80.